

Possibility of imaging lateral profiles of individual tetrahedral hybrid orbitals in real space

C Julian Chen

Institute of Applied Physics, Hamburg University, Jungiusstrasse 11, D-20355 Hamburg, Germany

Received 6 September 2005, in final form 31 January 2006

Published 10 March 2006

Online at stacks.iop.org/Nano/17/S195

Abstract

The imaging mechanism of scanning tunnelling microscopy (STM) and non-contact atomic force microscopy (NC-AFM) has the same origin, that is, the interaction between the electronic states of the tip and the electronic states of the sample. Therefore, using a well-characterized sample, the tip electronic states become the object to be probed by both STM and AFM. In this paper, we will present an analytic approach to compute the force distribution and the tunnelling-conductance distribution. As an example, we predict the possibility of resolving the lateral profiles of the tetrahedral hybrid orbitals, which are the foundation of many important materials essential to industry and life. We will discuss the conditions under which it could be observed, together with the issue of reproducibility.

1. Introduction

It was reported that while using NC-AFM to image a Si(111)7 × 7 surface, the image of the sp³ dangling bond on each adatom shows almost identical double-peak features [1]. The initial interpretation was the observation of two dangling bonds at the tip of the silicon tip [1, 2]. The validity of that interpretation was questioned [3, 4]. To date, apparently, the experiment has not been reproduced by other groups, and the nature of the observations has not been finally identified. Meanwhile, the electronic states of transition metal atoms are reported to be resolved by using silicon or graphite samples as probes in both AFM and STM [5, 6].

It is known that both covalent-bond force and tunnelling conductance are originating from the interaction between the electronic states of the tip and the electronic states of the sample [7]. Therefore, using a well-characterized sample, the tip electronic states could become the object to be probed. Because the electronic structure of the Si(111)7 × 7 surface is well understood, and the sp³ dangling bonds on the adatoms are well separated (about 0.7 nm), it is an ideal probe to study the electronic states at the end of the tip. Such a technique would open the possibility of imaging the subatomic structure of matter in real space, and would expand the frontier of the understanding of the atomic world.

To facilitate the interpretation of the AFM and STM images, in this paper we present an analytic method to

compute the force distribution and the tunnelling-conductance distribution. The basic idea is that the Bardeen surface integral, or the tunnelling matrix element, is also an accurate representation of the covalent-bond energy [7, 8]. Furthermore, within the muffin-tin approximation, the tunnelling matrix element can be evaluated analytically using the derivative rule. Therefore, the same analytic mathematical expression can be used to represent the force distribution and tunnelling-conductance distribution, and consequently, the NC-AFM image and the STM image. The normalization coefficients of the vacuum wavefunctions can be determined by the Hartree–Fock–Roothaan atomic wavefunctions [9]. As an example, we will make a prediction that it is possible to resolve the lateral profiles of tetrahedral hybrid orbitals, which are the foundation of many important materials essential to technology and life [10]. We will discuss the conditions under which those important elements could be observed, and the criteria to ascertain its validity.

2. Concept of tetrahedral hybrid orbitals

The concept of tetrahedral hybrid orbitals was introduced by Pauling and Slater [10] to explain the chemical bonding of methane and that like. The column 4A elements, such as carbon, silicon, and germanium, have four valence electrons in the outermost shell. Using the condition of maximum

directionality, Pauling showed that those atomic orbitals form four equivalent bond wavefunctions. The first one, along the z -direction, is [10]

$$\psi_1 = \frac{1}{2}s + \frac{\sqrt{3}}{2}p_z. \quad (1)$$

The second one, in the xz -plane, is

$$\psi_2 = \frac{1}{2}s - \frac{1}{2\sqrt{3}}p_z + \frac{\sqrt{2}}{\sqrt{3}}p_x, \quad (2)$$

and the third and fourth wavefunctions are

$$\psi_3 = \frac{1}{2}s - \frac{1}{2\sqrt{3}}p_z - \frac{1}{\sqrt{6}}p_x + \frac{1}{\sqrt{2}}p_y, \quad (3)$$

$$\psi_4 = \frac{1}{2}s - \frac{1}{2\sqrt{3}}p_z - \frac{1}{\sqrt{6}}p_x - \frac{1}{\sqrt{2}}p_y. \quad (4)$$

Those four orbitals are pointing to the four corners of a regular tetrahedron. Since those orbitals are formed by linear superposition of one s -type atomic orbital and three p -type atomic orbitals, those four localized and directed orbitals are often called tetrahedral hybrid orbitals, or sp^3 orbitals. Since their introduction in the late 1920s, the sp^3 orbitals have been the theoretical basis of the building process of many important materials, such as crystalline silicon and crystalline germanium, most of the carbon compounds as the basis of life, and diamond. However, to date, those sp^3 orbitals have been only in the theorist's mind, and they have never been perceived directly in real space.

To understand the concept of sp^3 orbitals quantitatively, in figures 1(a) and (b) we plot the absolute value of an sp^3 orbital of silicon. The parameters are taken from the Hartree–Fock–Roothaan atomic wavefunctions [9]. For simplicity, we use the single-zeta version of the atomic wavefunctions. Only the dominant Slater function is displayed. The $3s$ radial wavefunction is

$$\chi_{3s} = 51.86r^2e^{-3.09r}. \quad (5)$$

The $3p$ radial wavefunction is

$$\chi_{3p} = 32.34r^2e^{-2.70r}. \quad (6)$$

The sp^3 wavefunction in the z -orientation is

$$\psi = 7.31r^2e^{-3.09r} + 13.68rze^{-2.70r}. \quad (7)$$

The unit of length is the angstrom [9].

Here we show the absolute value of the wavefunction because the interaction energy of the covalent bond is related to the absolute value of the wavefunction [8]. The profile of the square of the wavefunction, the probability density, shows a similar feature.

In the following, we will show that it is possible to resolve the lateral profile of a single sp^3 orbital in real space, and thus to directly perceive the localized directed orbitals. This will provide a deeper understanding of the bonding process of a variety of materials which are important to technology as well as the understanding of life.

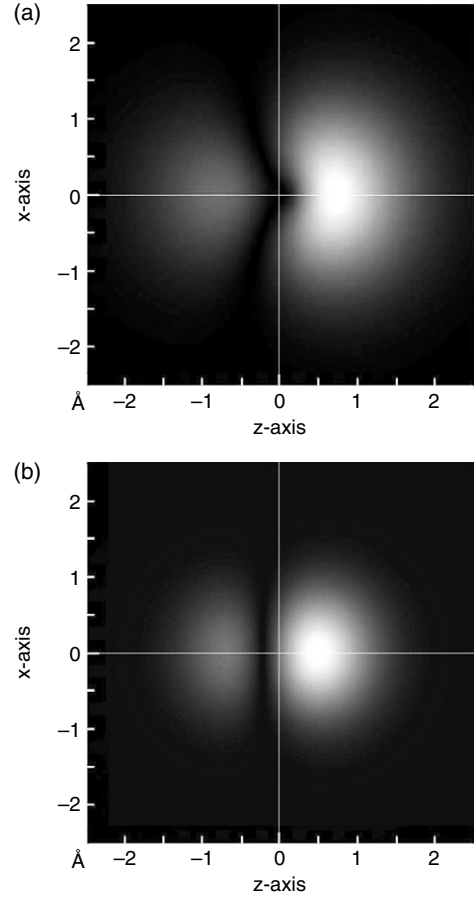


Figure 1. (a) The tetrahedral hybrid orbital of silicon at $y = 0$, showing the absolute value of the wavefunction. (b) The tetrahedral hybrid orbital of silicon at $y = 3 \text{ \AA}$, showing the absolute value of the wavefunction.

3. Experimental conditions

In the imaging process of STM and NC-AFM, for example, on a Si(111) 7×7 sample, a tip-sharpening procedure is often applied. When the atomic resolution is lost, by applying an electrical pulse or by controlled collision, atomic resolution can be resumed. It has been widely believed that during the tip-sharpening process, a Si atom or a small cluster of Si atoms is transferred from the sample surface to the tip. According to numerical simulations, various configurations of the silicon clusters could be formed [11]. The possible configurations of Si_4 and Si_5 clusters are shown in figure 2.

As an example, we consider the case of the bipyramidal Si_5 cluster, with two sp^3 orbitals on the two apices. When the cluster is formed on the tip end, it could have any orientation with respect to the tip axis. In general, the axis of the sp^3 orbital ζ can have an arbitrary angle γ with the norm of the sample surface z , as shown in figure 3.

From geometrical considerations, it is shown that the angle between the axis of the sp^3 orbital and a triangular plane of the tetrahedron is

$$\varphi = \arctan \frac{1}{2\sqrt{2}} = 0.3398 = 19^\circ 29'. \quad (8)$$

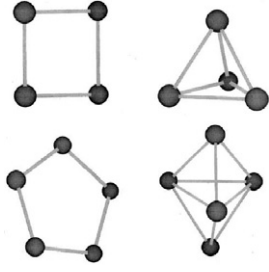


Figure 2. Possible configurations of silicon clusters. After [11].

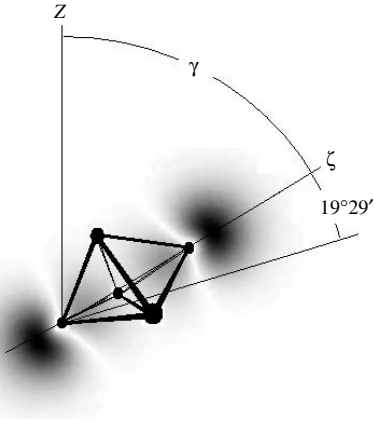


Figure 3. General configuration of an sp^3 orbital versus the norm of the sample surface, z .

The maximum angle between the norm of the sample and the axis of the sp^3 orbital is

$$\gamma_{\max} = 70^\circ 31'. \quad (9)$$

Thus, in principle, if the angle γ is large enough, the image of a single dangling bond at the adatom of the Si(111) 7×7 surface should split into a strong half-moon-shaped large feature, and a weak feature.

In the following, we make a detailed analysis of what images are expected, including both STM and NC-AFM.

4. Vacuum wavefunctions of sp^3 orbitals

The tunnelling current and atomic force can be calculated from the Bardeen tunnelling matrix element [7]. To do so, we need to know the wavefunctions of the sp^3 orbitals in the vacuum. Those wavefunctions are solutions of the following Schrödinger's equation,

$$(\nabla^2 - \kappa^2)\chi(\mathbf{r}) = 0. \quad (10)$$

The decay constant κ is defined by

$$\kappa^2 = \frac{2mW}{\hbar^2} \quad (11)$$

where m is the electron mass, and W is the workfunction. For Si(111), $W = 4.8$ eV, thus

$$\kappa = 1.117 \text{ \AA}. \quad (12)$$

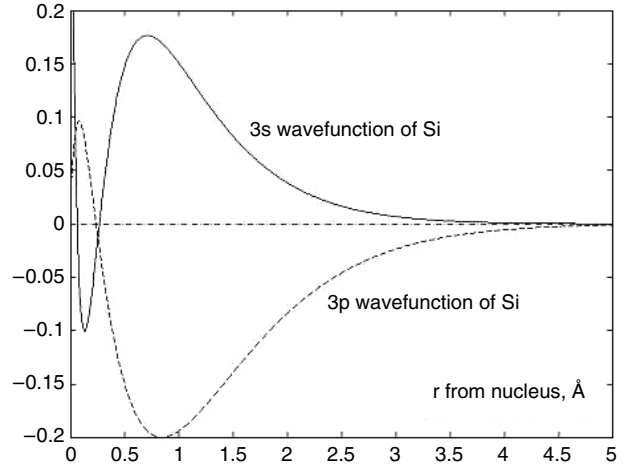


Figure 4. The Si 3s and 3p atomic wavefunctions computed using Hartree-Fock-Roothaan methods [9].

We look for wavefunctions in spherical coordinates (ρ, ϑ, ϕ) of the following form,

$$\chi(\mathbf{r}) = f_l(\rho)Y_{lm}(\vartheta, \phi). \quad (13)$$

As usual,

$$\rho = |\mathbf{r}| = \sqrt{x^2 + y^2 + z^2}. \quad (14)$$

Here, $Y_{lm}(\vartheta, \phi)$ is a spherical harmonic. For $f_l(\rho)$, equation (10) is reduced to

$$\frac{d}{d\rho} \left(\rho^2 \frac{df_l(\rho)}{d\rho} \right) - [\kappa^2 \rho^2 + l(l+1)] f_l(\rho) = 0. \quad (15)$$

For s-type and p_z -type wavefunctions, the spherical harmonics are

$$Y_{00} = \frac{1}{\sqrt{4\pi}}, \quad (16)$$

$$Y_{10} = \sqrt{\frac{3}{4\pi}} \cos \vartheta. \quad (17)$$

And the radial functions are modified spherical Bessel functions of the second kind [7],

$$f_0(\rho) = C_0 k_0(\kappa\rho) \equiv C_0 \frac{1}{\kappa\rho} e^{-\kappa\rho}, \quad (18)$$

$$f_1(\rho) = C_1 k_1(\kappa\rho) \equiv C_1 \left(\frac{1}{\kappa\rho} + \frac{1}{(\kappa\rho)^2} \right) e^{-\kappa\rho}. \quad (19)$$

The coefficients C_0 and C_1 are determined by comparing with first-principles calculations of atomic wavefunctions. Figure 4 shows the Hartree-Fock-Roothaan double-zeta Si 3s and 3p wavefunctions [9].

We fix the coefficients with the amplitudes of the wavefunctions at 2.5 \AA from the centre of the Si atom. The values thus obtained are

$$C_0 = 0.755 \text{ \AA}^{-3/2}, \quad (20)$$

$$C_1 = 1.545 \text{ \AA}^{-3/2}.$$

Combining with the spherical harmonics, using equation (1), the wavefunction of the first tetrahedral hybrid orbital in the vacuum is

$$\begin{aligned} \psi &= 0.107 k_0(\kappa\rho) + 0.654 k_1(\kappa\rho) \\ &\equiv 0.107 \frac{1}{\kappa\rho} e^{-\kappa\rho} + 0.654 \left[\frac{1}{\kappa\rho} + \frac{1}{(\kappa\rho)^2} \right] e^{-\kappa\rho} \cos \vartheta. \end{aligned} \quad (21)$$

Except for the orientation, the wavefunction of the tetrahedral orbital on the adatom of the Si(111)7 × 7 surface can be considered as the same.

Considering the angle of inclination γ , the wavefunction in the coordinate system with z -axis perpendicular to the sample surface is

$$\begin{aligned} \psi(\mathbf{r}) &= 0.107 \frac{1}{\kappa\rho} e^{-\kappa\rho} + 0.654 \left[\frac{1}{\kappa\rho} + \frac{1}{(\kappa\rho)^2} \right] \\ &\times \left[\frac{x \sin \gamma + z \cos \gamma}{\rho} \right] e^{-\kappa\rho}. \end{aligned} \quad (22)$$

5. Tunnelling matrix elements

Now we compute the tunnelling matrix elements using the derivative rule [7]. Using equation (22), we have

$$M = \frac{2\pi\hbar^2}{m\kappa} \left[0.107\psi(\mathbf{r}) + 0.654 \frac{\partial\psi(\mathbf{r})}{\kappa\partial z} \right]. \quad (23)$$

The calculation is straightforward but tedious. The result is

$$M = \frac{2\pi\hbar^2}{m\kappa} \{ \psi(\mathbf{r}) [0.107 + 0.654 f(\mathbf{r})] \}, \quad (24)$$

where

$$\begin{aligned} f(\mathbf{r}) &= -\frac{z}{\rho} - \frac{z}{\kappa\rho^2} + 6.11 \left\{ -\frac{z}{\kappa^2\rho^3} \left(\frac{x \sin \gamma + z \cos \gamma}{\rho} \right) \right. \\ &+ \left. \left(1 + \frac{1}{\kappa\rho} \right) \left[\frac{\cos \gamma}{\kappa\rho} - \frac{z}{\kappa\rho^3} (x \sin \gamma + z \cos \gamma) \right] \right\} \\ &\times \left\{ 1 + 6.11 \left(1 + \frac{1}{\kappa\rho} \right) \left(\frac{x \sin \gamma + z \cos \gamma}{\rho} \right) \right\}^{-1}. \end{aligned} \quad (25)$$

The force of chemical bonding in the z -direction is

$$F_z = -\frac{\partial|M|}{\partial z}, \quad (26)$$

and the tunnelling conductance for small bias is

$$G = \frac{(2\pi)^2 \rho_S \rho_T}{R_K} |M|^2. \quad (27)$$

In the following sections, we analyse the distribution of force and tunnelling conductance.

6. Force distribution

The force between the tip atom and the sample atom has three components: a slowly varying van der Waals force, the chemical bonding force (as a result of resonance as shown in the previous section), and the core–core repulsion. In the discussion of the fine profile of force distribution, we may

neglect the long-range weak van der Waals force. The core–core repulsion must be accounted for. The leading term of the attractive atomic force has the form

$$F_{\text{att}} \propto \frac{1}{\kappa z} e^{-\kappa z}. \quad (28)$$

Following the idea of the Morse curve, we assume that the repulsive component has the following form:

$$F_{\text{rep}} = C_0 \frac{1}{\kappa z} e^{-2\kappa z}. \quad (29)$$

The constant C_0 is determined by the condition that at the experimentally measured equilibrium distance in the bulk of Si, $z_0 = 2.35 \text{ \AA}$, the net force is zero. At a normal angle, the tunnelling matrix element is

$$\begin{aligned} M &= \frac{2\pi\hbar^2}{m\kappa} \left\{ 0.107 \frac{e^{-\kappa z}}{\kappa z} \left(7.11 + \frac{6.11}{\kappa z} \right) \left[0.107 \right. \right. \\ &+ \left. \left. 0.654 \left(1 + \frac{1}{\kappa z} + \frac{6.11}{(\kappa z)^2} \frac{1}{1 + 6.11(1 + 1/\kappa z)} \right) \right] \right\}. \end{aligned} \quad (30)$$

Putting the fundamental constants into equation (30), at $z_0 = 2.35 \text{ \AA}$ the attractive force is

$$F_{\text{att}} = -\frac{dM}{dz} \Big|_{z=z_0} \cong 7.23 \text{ nN}. \quad (31)$$

The value of C_0 is determined by using equations (29) and (30). We find

$$C_0 \cong 3616. \quad (32)$$

The total force (in nN) is then

$$F = -\frac{dM}{dz} + \frac{3616}{\kappa z} e^{-2\kappa z}. \quad (33)$$

Figure 5 shows the constant- z force distribution for a 65° inclination with a distance between the nucleus of the tip atom and the nearest sample atom of 3.0 \AA . The force distribution along the line $y = 0$ is shown in figure 6. In addition, the force distributions for $z = 3.5 \text{ \AA}$ and $z = 4.0 \text{ \AA}$ are also shown. As shown, the force contrast decreases rapidly with tip–sample distance.

7. Tunnelling-conductance distribution

The tunnelling conductance shows a similar feature. Figure 7 shows the tunnelling-conductance distribution for a 65° inclination angle at a tip–sample distance of 3.0 \AA . Figure 8 shows the values of tunnelling conductance at the $y = 0$ line.

As shown, the contrast of the tunnelling conductance is not as good as that of the force distribution. First, the force is proportional to the tunnelling matrix element, and the tunnelling conductance is proportional to the square of the tunnelling matrix element. Since the amplitude of the small lobe of the tetrahedral wavefunction is about one order of magnitude smaller than that of the large lobe, the square is two orders of magnitude smaller. Second, in the case of force, the repulsive force enhances the contrast between the two lobes. The tunnelling conductance is always positive. Therefore, the image looks like a deformed circle, instead of a well-defined double structure.

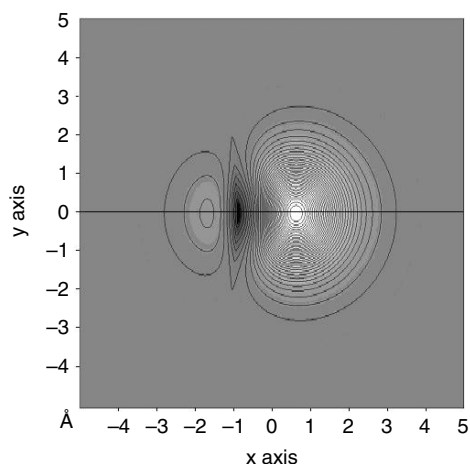


Figure 5. Force distribution of a tetrahedral hybrid bond, with a 65° inclination angle. The grey background indicates zero force. The light area indicates attractive force. The dark area indicates repulsive force. The distance between the nucleus of the tip atom and the nearest sample atom is 3 \AA .

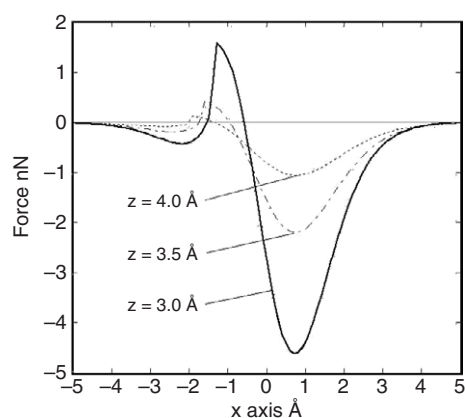


Figure 6. The force distribution along the x -axis, the white line in figure 4. In addition to the case of 3 \AA internuclear distance, the variation of the force curve with distance is also shown.

8. The issue of reproducibility

As we have discussed earlier, tip treatment is not a reproducible process. Every time a tip treatment procedure is executed, a new tip configuration is created. The appearance of a tetrahedral orbital is not a frequent event. It depends on the creation of a special tip structure. The concept of reproducibility is valid in a statistical sense. With a stable NC-AFM system, by using a computer-automated experiment to repeatedly treat the tip and then collect images, the entire collection of images should show statistical reproducibility. It is expected that a considerable percentage of the images does not show atomic resolution. Among the images with atomic resolution, the great majority of images should show a nearly spherically symmetric image for every dangling bond on the adatom of the Si(111) 7×7 surface. Nevertheless, there should be a small percentage of images showing nontrivial structures of the tip apex. Here the interesting physics would reside. In some sense, it is similar to the experiments in particle physics.

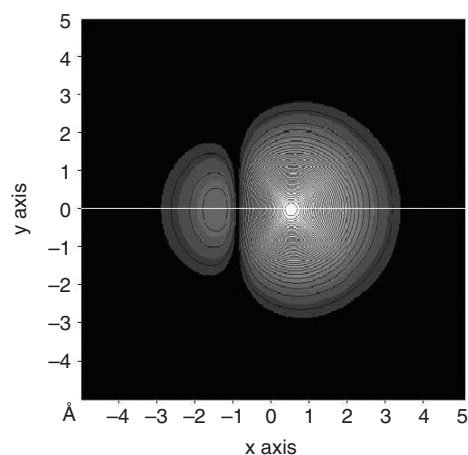


Figure 7. Tunnelling-conductance distribution of a tetrahedral hybrid bond, with a 65° inclination angle.

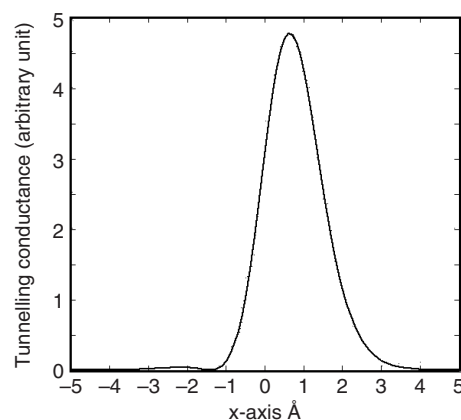


Figure 8. Tunnelling-conductance distribution of a tetrahedral orbital with a Si tip, along the line $y = 0$ in figure 7.

By recording and analysing a large number of events, exciting new physics would appear in a small fraction of the recorded events.

9. Conclusions

We have presented an analytic approach to compute the force distribution and the tunnelling-conductance distribution. As an example, we predict the possibility of resolving the lateral profiles of the tetrahedral hybrid orbitals, which are the foundation of many important materials essential to industry and life. We also discussed the conditions under which it could be observed, together with the issue of reproducibility.

Acknowledgments

This work is supported by the Deutsche Forschungsgemeinschaft. The author wishes to thank F J Giessibl for communicating recent experimental results, and numerous inspiring discussions. The author also thanks H Hölscher and V Caciuc for helpful discussions. Especially, the author thanks Professor

R Wiesendanger for inspiring discussions and careful reviewing of the manuscript.

References

- [1] Giessibl F J, Hembacher S, Bielefeldt H and Mannhart J 2000 *Science* **289** 422
- [2] Huang M, Cuma M and Liu F 2003 *Phys. Rev. Lett.* **90** 256101
- [3] Hug H J, Abdurixit M A, van Schendel P J A, Hoffmann R, Kappenberger P and Baratoff A 2001 *Science* **291** 2509
- [4] Giessibl F J, Hembacher S, Bielefeldt H and Mannhart J 2001 *Science* **291** 2509
- [5] Giessibl F J, Bielefeldt H, Hembacher S and Mannhart J 2001 *Ann. Phys. (Berlin)* **10** 887
- [6] Herz M, Giessibl F J and Mannhart J 2003 *Phys. Rev. B* **68** 45301
Hembacher *et al* 2004 *Science* **305** 380
- [7] Chen C J 1996 Unified perturbation theory of STM and SFM *Scanning Tunneling Microscopy* vol III, ed R Wiesendanger and H-J Güntherodt (Springer-Verlag) chapter 7
See also Chen C J 1993 *Introduction to Scanning Tunneling Microscopy* (New York: Oxford University Press)
- [8] Chen C J 2005 *Nanotechnology* **16** S27
- [9] Clementi E and Roetti P 1974 *At. Data Nucl. Data Tables* **14** 429
- [10] Pauling L 1931 *J. Am. Chem. Soc.* **53** 1367
- [11] Iwamatsu M 2000 *J. Chem. Phys.* **112** 10976